Annals of Biomedical Engineering, Vol. 42, No. 6, June 2014 (© 2014) pp. 1195–1206
DOI: 10.1007/s10439-014-1008-6

An *In Vitro* Evaluation of the Impact of Eccentric Deployment on Transcatheter Aortic Valve Hemodynamics

PAUL S. GUNNING,[1] NEELAKANTAN SAIKRISHNAN,[2] LAOISE M. MCNAMARA,[1] and AJIT P. YOGANATHAN[2]

[1]Biomechanics Research Centre, Department of Biomedical Engineering, National University of Ireland Galway, Galway, Ireland; and [2]Wallace H. Coulter Department of Biomedical Engineering, Georgia Institute of Technology and Emory University, Suite 232 Technology Enterprise Park, 387 Technology Circle, Atlanta, GA 30313, USA

(*Received 9 December 2013; accepted 31 March 2014; published online 10 April 2014*)

Associate Editor K. A. Athanasiou oversaw the review of this article.

Abstract—Patients with aortic stenosis present with calcium deposits on the native aortic valve, which can result in non-concentric expansion of Transcatheter Aortic Valve Replacement (TAVR) stents. The objective of this study is to evaluate whether eccentric deployment of TAVRs lead to turbulent blood flow and blood cell damage. Particle Image Velocimetry was used to quantitatively characterize fluid velocity fields, shear stress and turbulent kinetic energy downstream of TAVRs deployed in circular and eccentric orifices representative of deployed TAVRs *in vivo*. Effective orifice area (EOA) and mean transvalvular pressure gradient (TVG) values did not differ substantially in circular and eccentric deployed valves, with only a minor decrease in EOA observed in the eccentric valve (2.0 cm^2 for circular, 1.9 cm^2 for eccentric). Eccentric deployed TAVR lead to asymmetric systolic jet formation, with increased shear stresses (circular = 97 N/m^2 vs. eccentric = 119 N/m^2) and regions of turbulence intensity (circular = 180 N/m^2 vs. eccentric = 230 N/m^2) downstream that was not present in the circular deployed TAVR. The results of this study indicate that eccentric deployment of TAVRs can lead to altered flow characteristics and may potentially increase the hemolytic potential of the valve, which were not captured through hemodynamic evaluation alone.

Keywords—Transcatheter aortic valve implantation, Hemodynamics, Shear stress, Particle Image Velocimetry, Eccentric.

INTRODUCTION

Aortic stenosis (AS) causes progressive narrowing of the aortic valve, resulting in increased transvalvular pressure gradients (TVG), left ventricular hypertrophy and heart failure.[31] Transcatheter Aortic Valve Replacement (TAVR) is a percutaneous alternative to open heart surgery, which provides treatment of patients for whom conventional surgery is deemed unfeasible due to pre-existing illness or high risk of postoperative mortality.[31,35] TAVRs consist of animal derived tissue leaflets, which are mounted and crimped onto an expandable metallic frame and are delivered to the site of the native stenotic valve *via* a catheter through a transfemoral or transapical based approach. Once positioned correctly the valve stent expands radially and displaces the native stenosed valve into the aortic sinus.

Patients with AS typically present with large asymmetric calcium deposits on the native aortic valve, which vary in both size and density.[24,31,35] Conventional open-heart surgical techniques can remove the stenosed valve and calcium deposits to ensure optimal circular implantation of surgical valves.[31,35] Irregular calcium deposits and the native eccentric geometry of the annulus can restrict the deployment of the valve. This may lead to non uniform expansion of the stent, resulting in an eccentric geometry of the deployed TAVR.[6,40]

Balloon expandable and self expanding TAVRs exhibit favorable hemodynamic performance [effective orifice area (EOA), mean TVG] compared to surgical bioprosthesis.[8,13,47] Despite this, paravalvular leakage occurs in 65–89% TAVR patients[35] with aortic valve calcification and eccentric deployment proposed as the primary cause of leakage.[24,50] Nitinol stent designs have greater stent conformability than balloon expandable stents, to mitigate paravalvular leakage,[31,49] and thereby offer improved stent-aortic annulus apposition. However the conformance of the

Address correspondence to Ajit P. Yoganathan, Wallace H. Coulter Department of Biomedical Engineering, Georgia Institute of Technology and Emory University, Suite 232 Technology Enterprise Park, 387 Technology Circle, Atlanta, GA 30313, USA. Electronic mail: ajit.yoganathan@bme.gatech.edu

Nitinol stent to the calcified leaflets/annulus can exacerbate valve distortion and may lead to irregular leaflet kinematics.[40] It is not yet known whether distorted TAVR implantation geometries can alter leaflet kinematics sufficiently to cause non physiological flow patterns further downstream of the valve. Non physiological flow can lead to mechanically induced blood cell damage, which can be caused by prolonged exposure of blood cells to elevated shear stresses leading to hemolysis.[21,39] Previous studies have shown the existence of a threshold shear stress range of 150–800 N/m^2, above which blood cell damage can occur if subjected to for prolonged exposure times (min).[21,27,39] However the shear stresses arising downstream of an eccentric deployed TAVR have not yet been characterized. Although most TAVR patients are currently prescribed anti-thrombotic therapy, to prevent stroke or thromboembolic complications, a detailed understanding of the hemolytic potential of these devices is critical to facilitate the extension of this therapy to a wider patient population.

Flow assessment of TAVRs *in vivo* can be studied using transthoracic echocardiography (TEE). This modality however does not provide the required spatial and temporal resolution to assess the potential shear stress induced damage from eccentric deployed TAVRs. Additionally, multiple patient comorbidities may exist in high surgical risk patients that can complicate our understanding of the underlying mechanisms of shear stress related complications. *In vitro* bench-top testing allows for controlled parametric evaluation of the effects of valve implantation geometry on valve performance without the requirement for large cohort patient studies and eliminates other confounders, such as patient prosthesis mismatch and paravalvular leakage. Particle Image Velocimetry (PIV) is an optical based non-intrusive experimental technique, which can be used to evaluate flow fields through a prosthetic valve within a left heart simulator.[26,36,45] This technique allows for the examination of complex flow features such as vortices, regions of flow separation and stagnation.[26] More importantly, this Two Dimensional-Two Component (2D-2C) method has been extensively used to investigate shear stress and turbulent kinetic energy (TKE) quantities that can be used as a measure of the likelihood of blood damage.[1,2,26,36,37] However to date, PIV studies of TAVRs have been limited by focusing on flow through circularly deployed valves[14,36,38,45] and have not been applied to investigate flow alterations and hemolytic complications caused by non circular TAVRs deployed in heavily stenosed aortic valves *in vivo*.

In this study, we investigate the impact of eccentric TAVR deployment on turbulent flow formation, elevation of shear stresses and predict the potential for mechanically induced blood trauma downstream of the valve using an *in vitro* pulsatile left heart simulator and PIV techniques.

MATERIALS AND METHODS

Valve Model

A 23 mm supra annular TAVR design was studied, which has bovine pericardium leaflets sutured to a compressible and self-expanding Nitinol valve stent with dedicated commissure posts and an inflow segment.[35] Valve deployment was carried out as per clinical recommendation: once the supra annular portion of the valve stent was positioned correctly in the aortic root model (described below), lateral expansion of the inflow segment of the stent into the aortic root annulus was performed. Paravalvular leakage was mitigated through the use of a sealant around the valve circumference. The custom built idealized acrylic aortic root model based on clinical measurements[23,34] consisted of a straight rigid ascending aorta section developing into an axisymmetric sinus region and an interchangeable aortic annulus. Valves were deployed into two aortic annulus models: a circular control annulus (22 mm in diameter) and a severe asymmetric geometry ($D_{min} = 18.7$, $D_{max} = 25.8$) with an eccentricity index of 28% (eccentricity index $= (1 - D_{min}/D_{max})$), representative of highly eccentric explanted and *in vivo* TAVRs from CT imaging (Fig. 1a).[6,40]

Pulsatile Left Heart Simulator

The aortic root assembly was connected to the Georgia Tech Left Heart Simulator capable of simulating impaired and physiological hemodynamic conditions in an *in vitro* test setup, as shown in Fig. 1b. The pulsatile flow loop consisted of a fluid reservoir, a mechanical mitral valve, a bladder pump, an acrylic valve chamber, and compliance and resistance elements.[26,36,37] Ventricular function was simulated using a bladder pump driven by compressed air and solenoid valves. As the aortic root model was rigid, arterial dispensability was reproduced using a lumped systemic compliance chamber which was used to simulate flow conditions representative of normotensive pressure conditions (Mean Arterial Pressure = 100 mmHg) and a Heart Rate of 70 beats/min.[36,37] Cardiac output (CO), aortic and ventricular pressures were measured at 500 Hz using a custom Labview program. A blood analogue fluid of 36% water/glycerin solution was used in the experiments to simulate blood at a kinematic viscosity of 3.51e^{-6} m^2/s and minimize optical

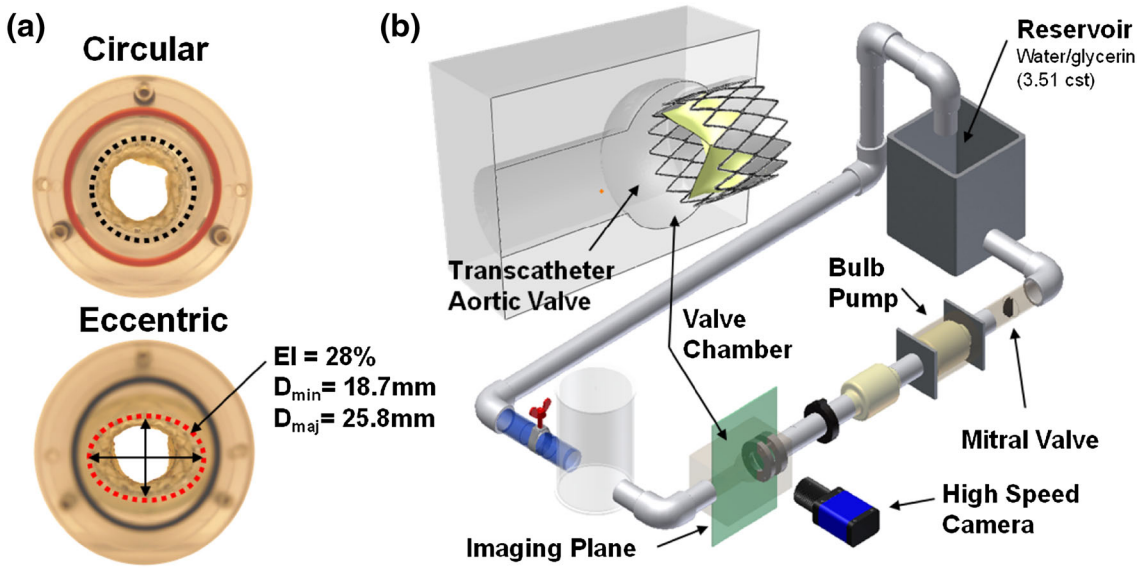

FIGURE 1. (a) Inflow morphologies of circular and eccentric deployed TAVRs with an eccentricity index = 28% and (b) pulsatile left heart simulator and PIV setup used to evaluate fluid flow through a TAVR.

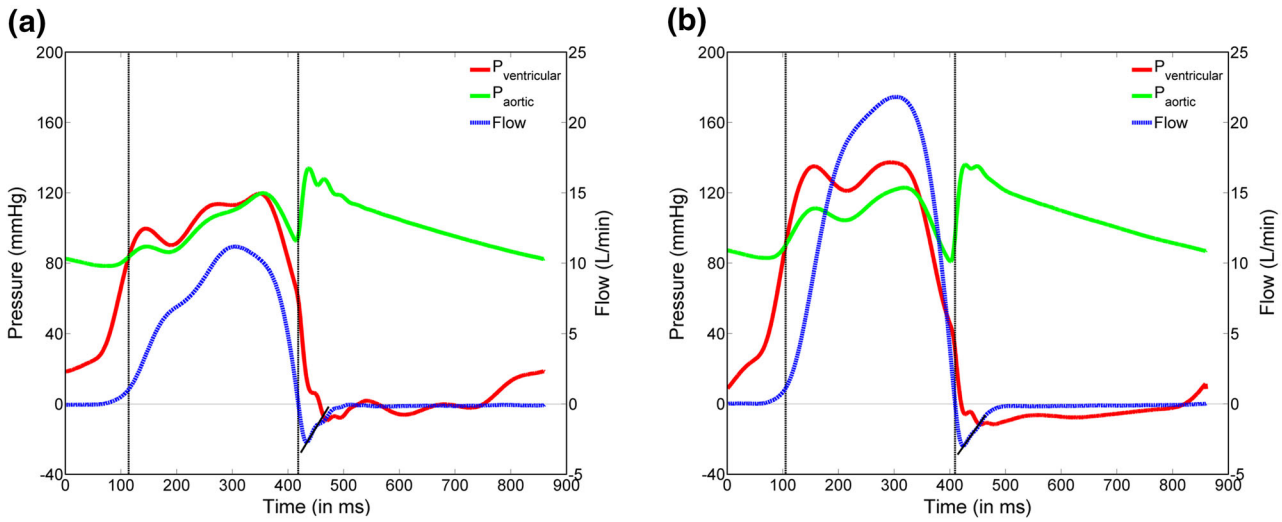

FIGURE 2. Hemodynamic waveforms including ventricular pressure (red line), aortic pressure (green line) and flow rate (blue dashed line) under (a) pathological flow conditions (CO = 2.5 L/min) analogous to patients with left ventricular and (b) physiological flow conditions (CO = 5.0 L/min).

distortion during flow analysis.[36,37] Valves were tested under two CO; an impaired pathological CO of 2.5 L/min, representative of patients with left ventricular dysfunction due to advanced stage AS,[9] and a physiological CO of 5 L/min.[36,37,51] Figures 2a and 2b show the resultant impaired and physiological waveforms acquired, which are similar to waveforms simulated in previous *in vitro* studies of native valves and TAVRs[36,37,51] and are also in accordance with ISO standards (ISO 5840—Cardiovascular implants—Cardiac valve prostheses).[5]

Particle Image Velocimetry

2D-2C PIV is a quantitative, optical based method of flow visualization which has been extensively used to study velocity and shear stress fields of aortic valve prosthesis in *in vitro* simulators.[2,28,36,37] 2D-2C PIV experiments were conducted on the deployed valve and aortic root assembly to generate ensemble averaged two dimensional velocity fields in the sinus and ascending aortic regions of the TAVR in both circular and eccentric deployments. The PIV system consisted of two

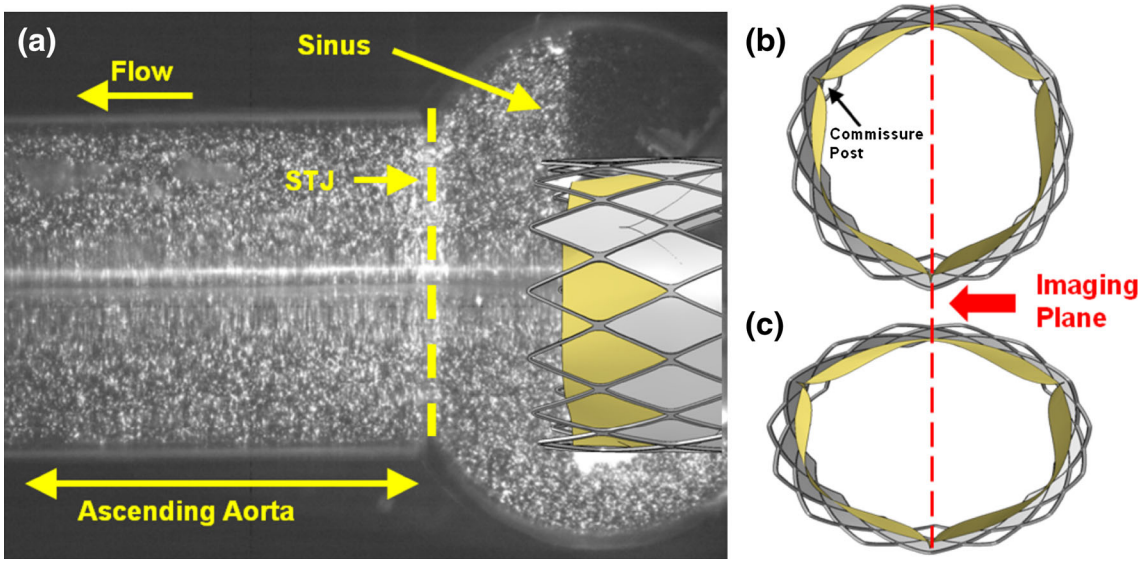

FIGURE 3. (a) Raw image of the particle laden fluid flow from the imaging plane. Idealized schematic of (b) circular and (c) eccentric deployed TAVRs at peak systole with imaging plane coincident with the lower commissure post and line of coaptation of the lower leaflets.

Nd:YAG pulsed lasers (ESI Inc., Portland, OR; 17 MJ energy, 532 nm wavelength, 9 ns pulse duration) used to illuminate polymethyl methacrylate (PMMA) particles (Dantec Dynamics, Denmark, Ø = 1–20 μm, emission at 580 nm) labeled with fluorescent Rhodium-D dye seeded in the fluid volume. A series of spherical/cylindrical lenses and mirrors were used to create a laser sheet of 1 mm thickness that illuminated the central plane of the valve assembly, as shown in Fig. 3a. The particles were imaged using a PIV CCD camera (LaVision, Germany, Imager Pro, 1600 × 1200 Px) with a Nikon Micro-Nikkor 60 mm lens and an orange filter with a resolution of 16.6 μm/pixel. Non linear optical calibration of the system was carried out to compensate for radial optical distortion caused by imaging through a curved surface, as well as refractive index mismatch between the blood analogue fluid ($n = 1.38$) and the acrylic aortic root model ($n = 1.49$).[36,37] Calibration was performed by placing a 2D calibration target with uniformly spaced dots coincident with the central imaging plane of the valve assembly. A 3rd order polynomial mapping function was fitted to the dots in the calibration image correcting the velocity vectors based on the distortion of the calibration target. Phase locked measurements of flow vectors were captured at 34 time points during the cardiac cycle separated by 25 ms. Time spacing (Δt) between laser pulses and image acquisition was optimized at each time point to ensure that the average displacement of particles between images was approximately 25% of the final interrogation window size.[22] As with previous studies, preliminary analysis showed that different Δt values did not produce any changes in ensemble averaged velocity fields, thus ensuring that the Δt chosen captured the large differences in flow velocity between ascending aorta and sinus regions.[36,37] Time spacing between laser pulses and image acquisition was optimized at each time point varying from 50 μs at peak systole to 1000 μs during the diastolic phase of the cardiac cycle.

At each acquisition time point, 200 image pairs were captured to enable averaging of flow fields to capture the most dominant flow structures and to obtain turbulence measurements. Images were post processed using DaVis 7.2 (LaVision, Germany) involving image pre-processing (background subtraction) and vector post processing to eliminate erroneous vectors arising from insufficient particle density and to recursively fill up empty regions of the vector field, as previously described.[36,37] Velocity measurements were acquired along the center line of the valve assembly, with the TAVR oriented such that one commissure post and line of leaflet coaptation was aligned with the imaging plane and the opposing leaflet was aligned perpendicular to the same plane (Figs. 3b and 3c). Moving leaflet boundaries during valve opening and closing were addressed by applying separate individual masks prior to vector calculation. A Matlab code (Mathworks, Natick, MA) was used to calculate additional Reynolds/Viscous Shear Stress and Turbulent Kinetic Energy quantities and visualized using Tecplot (Tecplot, Bellevue, WA).

Uncertainty Analysis

Uncertainty analysis was conducted to calculate bias errors in the PIV system, which may be caused by pixel displacement gradients and time spacing between

TABLE 1. Maximum and minimum velocity uncertainty measurements during the diastolic and systolic durations of the cardiac cycle at CO of 2.5 and 5.0 L/min.

Time point	Δt (μs)	Max and min velocity uncertainty (m/s)
CO = 2.5 L/min		
Diastole	500–1000	0.0017–0.0066
Systole	125–300	0.0055–0.0262
CO = 5.0 L/min		
Diastole	500–1000	0.0017–0.0066
Systole	75–200	0.0082–0.0437

laser pulses.[10,33] Velocity uncertainty was calculated as the smallest measureable displacement divided by the time spacing at each acquisition point. The maximum and minimum velocity uncertainty (m/s) at each acquisition in the cardiac cycle is shown in Table 1. Peak velocity uncertainty occurred at 300 ms into the cardiac cycle, which was approximately 1.7% of the maximum velocity at this acquisition point. In addition to bias errors, precision errors related to repeatability may be present, which cannot be quantified due to turbulent fluctuations but are intrinsic in pulsatile flow with mid to high Reynolds number.[36] Therefore it is not possible to isolate cycle-to-cycle variation of the loop. Despite this, ensemble averaging of 200 vector fields is sufficient in obtaining statistically converged values for the calculated quantities defined below. For our PIV experiments, only 1 TAVR was used. Therefore it was not possible to calculate the effect of valve-to-valve variability on the results obtained. However as the valve used was manufactured to clinical standards we expect valve-to-valve variability to be minimal.

Definition and Clinical Relevance of Calculated Quantities

Effective Orifice Area and TVG

Hemodynamic performance of the valves evaluated using TVG and EOA. TVG values were calculated as the mean pressure gradient (ΔP_{mean}) across the valve during systole, while EOA values were calculated using the root mean square of the measured flow (Q_{rms}) as in the following equation.

$$\text{EOA} = \frac{Q_{\text{rms}}}{51.6\sqrt{P_{\text{mean}}}}$$

Values were acquired over 15 cardiac cycles and then averaged to get representative data for circular and eccentric deployed valves.[53]

Velocity Vectors

Velocity vectors allow for the visualization and measurement of flow patterns in the immediate vicinity and downstream of the valve. Velocity vectors can be used to examine complex flow structures such as vortices, regions of flow separation, stagnation and turbulence as well as areas of ineffective washout in the vicinity of the valve stent, which can be correlated to locations of thrombus formation.[26] The magnitude of velocity vectors were derived using the following formula $\text{Vel}_{\text{Magnitude}} = \sqrt{U^2 + V^2}$, where U and V are instantaneous velocities in the X and Y directions.

Reynolds/Viscous Shear Stresses and TKE Fields

Reynolds and Viscous shear stress quantities have been correlated to blood cell damage and turbulence and can serve as a predictor of likely areas where hemolysis may occur.[15,37] Reynolds shear stresses (RSS) are a statistical quantity measuring shear stresses between layers of fluid flow caused by temporal variations in the velocity field, which can form due to cycle-to-cycle variations as well as fluctuations in turbulent flow. RSS values are calculated using the following equation:

$$\text{RSS} = \rho\sqrt{\left(\frac{\overline{u'u'} - \overline{v'v'}}{2}\right)^2 + \left(\overline{u'v'}\right)^2},$$

where ρ is the density of the blood analogue fluid and $\overline{u'}$ and $\overline{v'}$ are the mean instantaneous velocity fluctuations in the X and Y directions. Fluctuations in the velocity field were calculated by subtracting the mean velocity from the instantaneous velocity at each acquisition point in the cardiac cycle. Mean velocity fields were determined by averaging 200 velocity fields at each timepoint. Peak RSS occur in boundary layers between high velocity flow interacting with quiescent fluid and can indicate regions of turbulent flow.[15,37]

Viscous shear stresses (VSS) are a measure of the instantaneous shear load between layers of fluid and can be related to the physical forces acting on blood constituents from the surrounding fluid volume.[15,37] VSS values are calculated using the following equation:

$$\text{VSS} = \mu\left(\frac{dU}{dx} + \frac{dV}{dy}\right),$$

where μ is the kinematic viscosity of the blood analogue fluid.[37]

Turbulent kinetic energy (TKE) is the kinetic energy of eddies in the fluid volume and can be used as a measurement of turbulence intensity.[37] TKE was calculated using this equation:

$$\text{TKE} = \frac{1}{2}\left(\overline{u'^2} + \overline{v'^2}\right)$$

Turbulent flow combined with extended exposure of cells to elevated shear stresses can result in rupture of

the cell membranes, release of cell contents and lead to platelet aggregation and thrombolic events.[25,52]

RESULTS

Hemodynamic Performance

Typical hemodynamic waveforms of the circular and eccentric deployed TAVRs at impaired (2.5 L/min) and physiological (5 L/min) CO are shown in Figs. 2a and 2b. The circular implanted valve had a lower mean TVG than the eccentric deployed valve at both 2.5 L/min (2.4 vs. 2.72 mmHg) and 5 L/min CO (6.9 vs. 8.0 mmHg). A higher EOA was reported for the circular valve than the eccentric valves at both impaired CO (1.8 vs. 1.7 cm^2) and physiological CO (2.0 vs. 1.9 cm^2).

Vector Velocity Fields

Results described in this section are shown in Fig. 4 and relate to averaged flow fields at different stages during systolic ejection and diastole at locations downstream of the TAVR at pathological and physiological CO: Early Systole (175 ms), Peak Systole (300 ms), Late Systole (375 ms) and Diastole (500 ms).

During early systole (175 ms), accelerating flow emanated from the central orifice of both valves, see Fig. 4. At physiological CO, a central systolic jet was observed in the circular deployed valve with a peak velocity of 0.8 m/s that started to converge to a point further downstream at the sinotubular junction (STJ). In the eccentric deployed valve, a narrow, offset and accelerated jet occurred with a peak velocity of 1.5 m/s, which developed into a divergent flow at the STJ with a low velocity vortex ring appearing around the jet that impinged on the STJ and caused flow reversal into the lower sinus region. Similar flow profiles were observed at the impaired CO, however the systolic jets did not extend into the ascending aorta due to the lower instantaneous flow rate.

At peak systole (300 ms) at physiological CO peak velocities of 2.57 and 2.45 m/s occurred in the circular and eccentric deployed valves respectively. In the circular deployed valve, the systolic jet had a flat velocity profile in the immediate vicinity of the open valve that further developed into a high velocity convergent central jet further downstream. In the eccentric deployed valve, an asymmetric jet occurred resulting in the upward deviation of the systolic jet from the center line of the ascending aorta. In addition to this a vortex formed below the jet impinging on the STJ that was not present in the circular deployed valve. At the impaired CO, similar systolic jet formation occurs in both deployed valves, however the asymmetric jet formation is less pronounced in the eccentric valve at this CO.

At late systole (375 ms), flow started to decelerate caused by pressure reversal in the aorta. Flow characteristics remain consistent with peak systole with velocities reducing with CO, $Vel_{Peak} = 1.1$ m/s at CO = 2.5 L/min and $Vel_{Peak} = 1.9$ m/s at CO = 5 L/min recorded in both deployed valves. At late systole and early diastole, pressure reversal causes the movement of fluid flow along the aortic wall towards the sinus region. Minimal flow velocities are observed in the sinus region due to the supra annular implantation characteristics of the valve.

At diastole (500 ms), following valve closure, the flow velocities were approximately zero in all valve models at each CO. Quiescent flow showed no regurgitant flow following valve closure, indicating that correct leaflet coaptation and no central valvular leakage occurred irrespective of valve geometry.

Reynolds/Viscous Shear Stresses and TKE Fields

During systole, flow accelerates from the valve into quiescent fluid in the ascending aorta. At peak systole, where the highest jet velocities occur, a shear layer forms between the fast moving fluid in the systolic jet and the slow moving quiescent fluid in the aorta. In circular deployed valves, RSS values ranging between 30 and 97 N/m^2 were found at the interface of the accelerated systolic jet and the quiescent stagnant fluid in the aorta at both CO, see Fig. 5. A high magnitude region of RSS of 97 N/m^2 was found in the flow emanating from the stent post in the lower half of the chamber. In the eccentric deployed valve regions of high RSS coincided with high velocity gradients regions, reaching values up to $RSS_{Peak} = 119$ N/m^2 at 5.0 L/min located in turbulent region below the trailing edge of the systolic jet that was not present in the circular deployed valve.

In the VSS profiles (Fig. 5), maximum and minimum VSS values were the same for both valve deployments at each CO ($VSS_{Max} = 2.5$ N/m^{-2} and $VSS_{Min} = -2$ N/m^{-2} at 2.5 L/min CO, $VSS_{Max} = 4$ N/m^{-2} and $VSS_{Min} = -5$ N/m^{-2} at 5 L/min CO). In the circular deployed valves regions of positive and negative VSS are parallel to one other and are closer together under pathological flow conditions which is indicative of the lower EOA observed at this CO. In contrast to this, the leading edge of these maximum and minimum regions of VSS in the eccentric deployed valves are deviating from each other with a more divergent VSS profile observed at the higher CO that nearly impinges on the STJ.

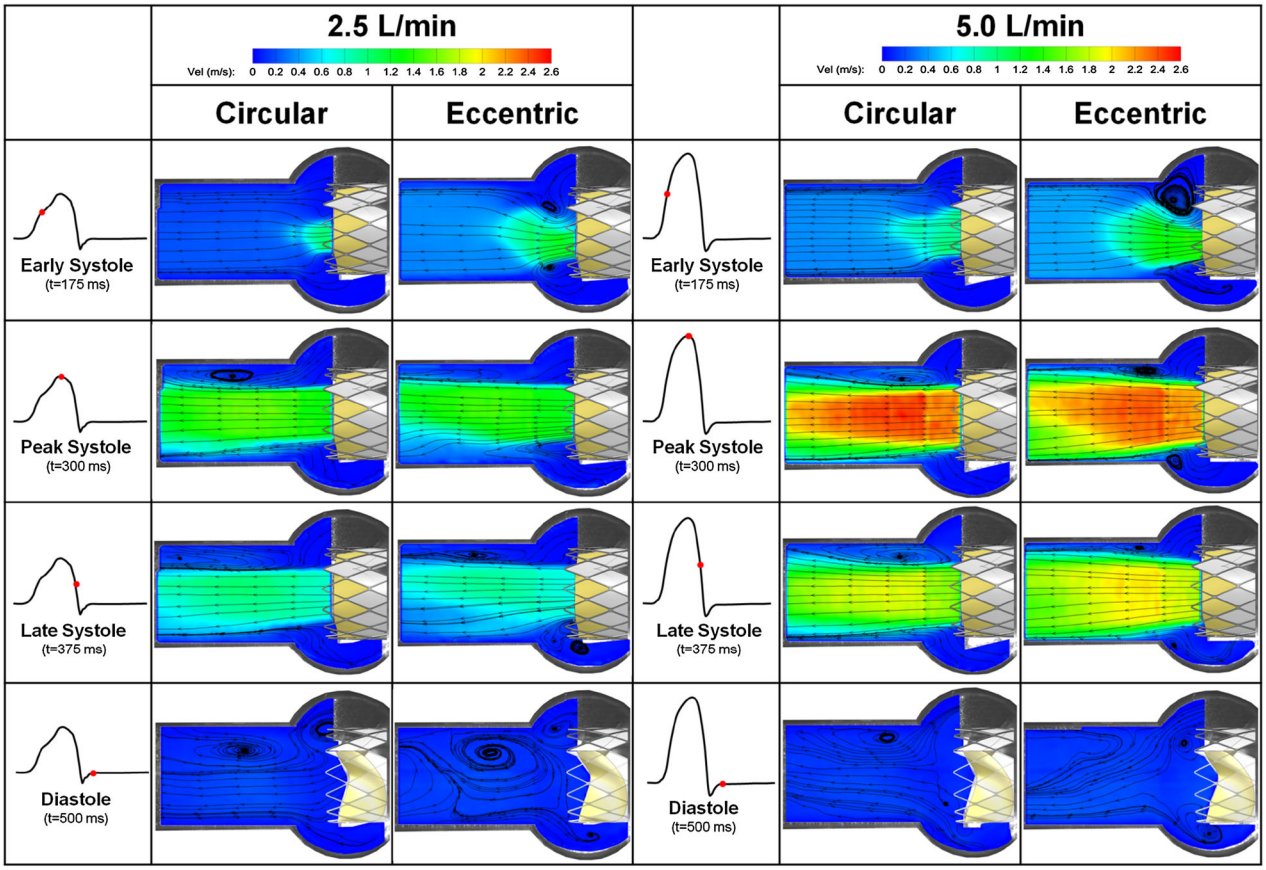

FIGURE 4. Velocity vector profiles at pathological and physiological CO in valves deployed in circular and eccentric orifices at early, peak and late systole (flow going from right to left).

For both deployment geometries, areas of elevated TKE occurred at the boundaries of the systolic jet. In the circular valve, flow with an elevated TKE occurred close to the stent post and continued downstream of the valve with a peak value of 180 N/m^2 at CO = 5 L/min and 120 N/m^2 at 2.5 L/min. In the eccentric deployed valves, higher TKE values (230 N/m^2) occurred at both CO's and were observed in a localized pocket below the edge of the deviated systolic jet. This pocket was not present in the circular deployed valve, see Fig. 5.

DISCUSSION

This study provides a comprehensive comparison of the flow characteristics of circular and eccentric deployed TAVRs using an *in vitro* left heart simulator and PIV. Our results show that EOA and mean TVG gradients did not differ substantially between circular and eccentric deployed TAVRs. Despite this, the eccentric deployed TAVR lead to asymmetric systolic jet formation, with elevated turbulence and shear stress downstream of the valve, which was not present in the circular deployed TAVR.

Mean TVG and EOA are performance criteria commonly used to compare hemodynamics of prosthetic valve designs. Our results show that EOA and mean TVG values did not differ substantially in circular and eccentric deployed valves and were within the range reported for other TAVRs designs *in vitro*[36] and *in vivo*.[11,12,44] Examination of EOA and mean TVG metrics from this study alone would imply that eccentric deployment of TAVRs has a minor impact on valve performance. However, further analysis of the flow development was performed here to study the alterations in systolic jet formation that may occur due to eccentric implantation. It was observed that, although the peak velocity was lower in the eccentric valve compared to the circular valve, a region of elevated shear stresses occurred in a localized pocket under the trailing edge of the offset systolic jet with an increased peak shear stress than that occurring in the circular valve (119 N/m vs. 97 N/m^2). It must be noted that these shear stresses remained marginally below the threshold range of 150–800 N/m^2 at which hemolysis can occur.[21,27,39] This region coincided with an area of elevated peak turbulence intensity (230 N/m^2) that was not present in the circular deployed valve (180 N/m^2).

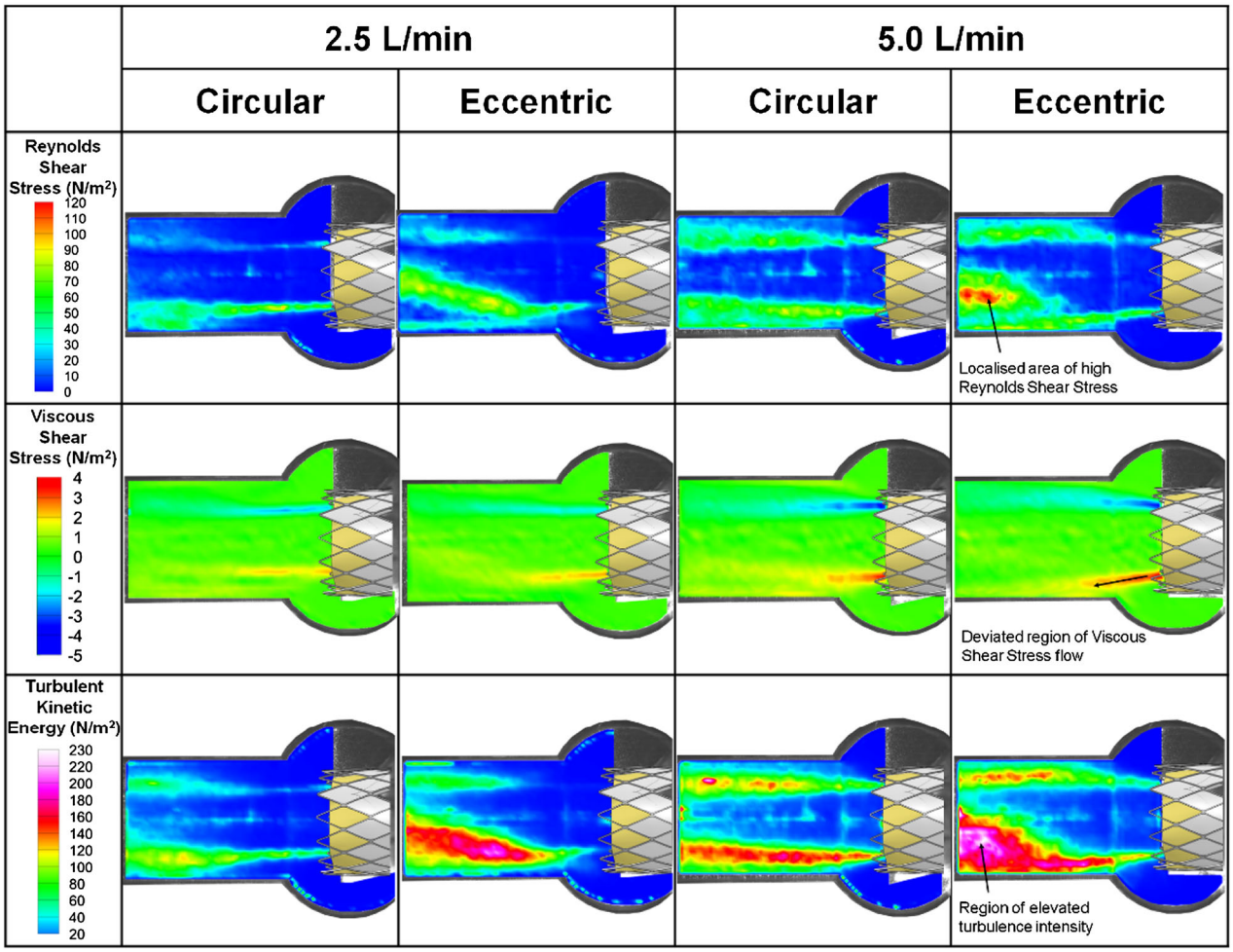

FIGURE 5. Reynolds shear stress, viscous shear stress and turbulent kinetic energy plots at pathological and physiological CO at peak systole (flow going from right to left).

Therefore, despite similar hemodynamic performance of both valve configurations, the findings of this study show that eccentric valve deployment can result in asymmetric systolic jet formation with elevated turbulence and shear stress downstream of the valve, however these may not be sufficient to induce blood damage.

The primary limitation in our study was the use of a rigid idealized aortic root model. This model does not represent the compliant behavior of the aortic tissue or undergo changes in annulus shape that occur *in vivo*.[4] Rigidity of the aortic wall may increase fluid velocities and inhibit the dissipation of vortices downstream compared to a more compliant wall model.[7,48] However calcium deposits,[20] age related reduced arterial compliance[7] in patients requiring TAVR and the scaffolding provided by over-sizing of the valve may reduce compliance and dimensional changes of the aortic root *in vivo* and as such a rigid model was deemed appropriate. A calcified native valve was not included in the aortic root model. However the circular and eccentric aortic annuli geometries chosen were representative of *in vivo* TAVR deployment geometries from CT imaging.[6,40] The axisymmetric sinus geometry is not representative of a typical three lobed sinus found *in vivo* which has recently been shown to aid in increasing valve EOA.[32] Despite this however, the dimensions have been designed to match anatomical measurements[23,34] and although simplified, is still capable of capturing flow fields in the sinus region associated with the upper leaflet in the valve model. In addition to this, the TAVR in question is in a supra annular position, which reduces the distance between the STJ and the TAVR leaflets.[38] As a result, movement of fluid into the sinus region is inhibited[38] thus minimizing the impact of the axisymmetric geometry on the results of the study. Flow characterization was carried out in the plane of the minor axis of the ellipse only, which was chosen as the most severe condition as the valve diameter is reduced by 4.3 mm compared to

the circular valve. In addition to this, the plane studied is coincident with the distorted stent post allowing for the capture of deviated flow caused by eccentric deployment. Moreover, a previous study has shown peak shear stresses occur at this plane and decrease in magnitude in offset planes.[37] The 2D-2C PIV analysis used did not permit for the measurement of out of plane components of the calculated quantities. However strong axial flow downstream of the valve is much more dominant in this plane, compared to transverse components of the flow[28] and our results confirmed this through low out of plane particle loss observed in the processed flow field images.[2,36] Thus a two dimensional flow analysis can approximate this flow relatively accurately and has been widely applied in studies of native and prosthetic valves.[1,28,36,37] In addition to shear stress magnitude and exposure time, red blood cell (RBC) hemolysis and platelet lysis/activation are also dependent upon shear stress history. Previous studies have used empirical based mathematical models to investigate cell shear stress history and the effect of sublethal damage accumulation of blood constituents.[16–18,30] Previous CFD and 2D-2C PIV studies have used Lagrangian particle tracking for the calculation of the exposure duration and loading history of fluid particles in flow fields downstream of prosthetic valves.[2,28,43] The addition of particle tracking and empirical modeling in estimation of damage accumulation is beyond the scope of this current study and may be investigated in the future to further relate flow field abnormalities to the thrombogenic potential of non-concentric TAVRs. Finally, the TAVR used in this study is based on a unique supra annular design concept that minimizes the effect of stent asymmetry at the valvular segment of the TAVR. We propose that eccentric deployment will exacerbate distortions at valvular levels in other TAVR designs, but future studies are required to investigate this further.

The observed flow fields through the circular deployed valve reported here have the same characteristics as flow through native and bioprosthetic valves reported in previous studies, with a central high velocity jet symmetrical about the central axis of the valve.[37,45] The peak velocities reported here (~2.5 m/s) are significantly higher than that of the 23 mm Edwards Sapien TAVR[45] (0.85 m/s) but are comparable to the peak velocity reported for native[37] (~2.8 m/s), polymeric[26] (~2.55 m/s) and other TAVRs[29,36,38] (2.1–2.3 m/s) under similar *in vitro* and *in vivo* hemodynamic conditions. Typically, self expanding TAVRs are deployed undersized in order to produce sufficient radial force to prevent valve migration.[46] This in conjunction with the tapered midsection characteristics of the valve stent studied here, reduces orifice area and increases peak flow velocities compared to other TAVR designs.[29,36,38,45] In the eccentric valve, the asymmetric systolic jet observed may be a 2D cross section of a helical flow pattern in 3D, which is synonymous with observed flow fields *in vivo*.[33,34] It is expected that helical flow occurs in both valve geometries, however occurs earlier downstream of the eccentric valve, due to the presence of a pocket of elevated TKE under the systolic jet, and thus is captured in the field of view of this valve. However for the circular valve this transition occurs further downstream, which is out of the field of view of the PIV experiment. The increase in turbulence intensity likely arises due to stent distortion, which causes the stent posts to move radially outwards causing deviation of flow in the lower half of ascending aorta towards the aortic wall resulting in an area of flow recirculation and elevated turbulence. The formation of helical flow in the eccentric valve serves as a method to minimize the TKE in the flow by inducing rotational stability and thereby mitigating the transition to turbulent flow.[33,34] *In vivo*, this has been shown in flow profiles post TAVR, whereby a strong asymmetric jet was formed that transitioned into helical flow early in the ascending aorta.[29] However, it must be noted that in order to gain a further insight in helical flow patterns arising from valve eccentricity, analysis of the flow field in 3 dimensions may be investigated.

Mechanically induced blood damage is dependent upon both the magnitude and the length of exposure of blood constituents to abnormal shear stresses. Shear stress values ranging from 150 to 800 N/m^2 are accepted as the threshold range at which onset of RBC hemolysis can occur.[21,27,39] Once in this range the degree of hemolysis is a function of the shear stress magnitude and the exposure time ($10e^{-3}$–10^2 s).[21,27,39] Although we found increased shear stress in the eccentric valve (compared to the circular valve), we report that the values are lower than this threshold.[21,27,39] This increase in RSS occurs due to the separation of flow in the developing asymmetric jet resulting in turbulent mixing occurring. At the higher CO, this is exacerbated and higher fluctuating shear stresses result. As asymmetric flow is not observed in the field of view of the circular valve, turbulent mixing is not captured and an increase in RSS with CO is not observed. Previous studies have investigated blood damage below this threshold region and have shown that at a shear stress level below 150 N/m^2, levels of hemolysis per unit time are relatively low and mechanically induced blood damage is therefore unlikely.[3,27,41] In addition to this, the region of peak RSS in the eccentric valve was coincident with an area of high flow velocity (1.8–2.1 m/s), suggesting that cells in this area experience peak RSS for a short duration before continuing further downstream. Although we

have found that the elevated shear stress magnitudes are not in the range for which blood damage can occur, our findings do show that shear stress values did increase with CO, an increase that did not occur in the circular deployed valve. An increase in CO caused by exercise or cardiac arrhythmia may potentially further increase shear stress into the threshold range and increase the blood damaging potential of flow caused by eccentric valve deployment and as such these findings warrant further investigation.

Unlike RBC, platelets are more sensitive to shear stresses, with viscous shear stresses of 10 N/m^2 been shown to cause platelet lysis.[19] Our results show that, despite RSS values increasing for an eccentric deployed TAVR, the instantaneous VSS remain the same for both circular and eccentric geometries. Despite not exceeding the critical shear stress for platelet activation, VSS values are close to 6 N/m^2, which has been shown to be a sublethal shear stress threshold at which platelets can become sensitized and are 20 times more likely to be activated in subsequent low shear flows.[42] This is significant in the TAVR studied here, whereby the distorted geometry directs high VSS flow (5 N/m^2) towards the STJ and sinus regions. Stagnant flow in the sinus may expose sensitized platelets to extended exposure time of low shear stress making this site prone to thrombus formation.[42]

CONCLUSION

In this study we compare the flow alterations caused by eccentric deployment of a TAVR and provide an insight in the clinical complications that may be caused by non-concentric deployment. Our findings show that typical performance metrics (EOA and TVG) did not differ substantially between circular and eccentric deployed TAVRs. Despite this, significant changes in systolic jet formation in the eccentric TAVR was observed, with elevated regions of turbulence intensity (230 N/m^2) and shear stress (120 N/m^2), which are not present in circular deployed valves (180, 97 N/m^2). It was found that eccentric deployment of the TAVR resulted in distorted stent geometry at the outflow segment of the valve, causing flow deviation towards the aortic wall and asymmetric flow formation compared to the circular valve. Although the increased shear stresses caused by eccentric deployment were not high enough to cause blood damage, increased shear stress values were only marginally below the threshold range for which hemolysis may occur. Viscous shear stress magnitudes (5 N/m^2) were found to be close to a threshold value for sensitisation of platelets can occur (6 N/m^2) which in conjunction with the an eccentric deployment geometry may lead to extended exposure times and thrombus formation. In addition to this, the results of this study can provide input into studies which can further elucidate the impact of altered flow characteristics of asymmetric TAVRs on mechanobiological responses *in vivo*. As the clinical use of TAVRs increase with the introduction of new valve technologies, imaging modalities and younger patient populations, the assessment and understanding of TAVR performance in asymmetric geometries is critical in determining the successful implantation of TAVR in patients with wide ranging aortic root morphologies.

ACKNOWLEDGMENTS

The authors would like to acknowledge the assistance from the Georgia Tech Research Institute (GTRI) machine shop for manufacturing the acrylic models used in the study. This study was funded by the Science Foundation Ireland Short Term Travel Fellowship Award, a National University of Ireland Galway (NUI Galway) College of Engineering and Informatics Fellowship and the Wallace H. Coulter endowment fund to A. P. Yoganathan.

CONFLICT OF INTEREST

None.

REFERENCES

[1]Bellofiore, A., E. Donohue, and N. Quinlan. Scale-up of an unsteady flow field for enhanced spatial and temporal resolution of PIV measurements: application to leaflet wake flow in a mechanical heart valve. *Exp. Fluids* 51:161–176, 2011.

[2]Bellofiore, A., and N. Quinlan. High-resolution measurement of the unsteady velocity field to evaluate blood damage induced by a mechanical heart valve. *Ann. Biomed. Eng.* 39:2417–2429, 2011.

[3]Blackshear, P. L. Hemolysis at Prosthetic Surfaces. In: Chemistry of Biosurfaces, edited by M. L. Hair. New York: Marcel Dekkar, 1972, pp. 523–562.

[4]Blanke, P., M. Russe, J. Leipsic, J. Reinöhl, U. Ebersberger, P. Suranyi, M. Siepe, G. Pache, M. Langer, and U. J. Schoepf. Conformational pulsatile changes of the aortic annulus: impact on prosthesis sizing by computed tomography for transcatheter aortic valve replacement. *J. Am. Coll. Cardio. Interv.* 5:984–994, 2012.

[5]Cardiovascular Implants—Cardiac Valve Prostheses ISO 5840. ISO, Geneva, Switzerland, 2005.

[6]Cavero, M. A., J. Goicolea, C. García-Montero, and J. F. Oteo. Prognostic implications of asymmetric morphology in transcatheter aortic valve implantation: a case report. *Rev. Esp. Cardiol.* 65:104–105, 2012.

[7]Cecelja, M., and P. Chowienczyk. Role of arterial stiffness in cardiovascular disease. *JRSM Cardiovasc. Dis.* 1:1–11, 2012.

[8]Clavel, M.-A., J. G. Webb, P. Pibarot, L. Altwegg, E. Dumont, C. Thompson, R. De Larochellière, D. Doyle, J.-B. Masson, S. Bergeron, O. F. Bertrand, and J. Rodés-Cabau. Comparison of the hemodynamic performance of percutaneous and surgical bioprostheses for the treatment of severe aortic stenosis. *J. Am. Coll. Cardiol.* 53:1883–1891, 2009.

[9]Connolly, H. M., J. K. Oh, T. A. Orszulak, S. L. Osborn, V. L. Roger, D. O. Hodge, K. R. Bailey, J. B. Seward, and A. J. Tajik. Aortic valve replacement for aortic stenosis with severe left ventricular dysfunction: prognostic indicators. *Circulation* 95:2395–2400, 1997.

[10]Cooper, B. T., B. N. Roszelle, T. C. Long, S. Deutsch, and K. B. Manning. The 12cc Penn State pulsatile pediatric ventricular assist device: fluid dynamics associated with valve selection. *J. Biomech. Eng.* 130:041019, 2008.

[11]Cribier, A., H. Eltchaninoff, C. Tron, F. Bauer, C. Agatiello, D. Nercolini, S. Tapiero, P.-Y. Litzler, J.-P. Bessou, and V. Babaliaros. Treatment of calcific aortic stenosis with the percutaneous heart valve: mid-term follow-up from the initial feasibility studies: the French experience. *J. Am. Coll. Cardiol.* 47:1214–1223, 2006.

[12]Cribier, A., H. Eltchaninoff, C. Tron, F. Bauer, C. Agatiello, L. Sebagh, A. Bash, D. Nusimovici, P. Y. Litzler, J.-P. Bessou, and M. B. Leon. Early experience with percutaneous transcatheter implantation of heart valve prosthesis for the treatment of end-stage inoperable patients with calcific aortic stenosis. *J. Am. Coll. Cardiol.* 43:698–703, 2004.

[13]D'Errigo, P., M. Barbanti, M. Ranucci, F. Onorati, R. D. Covello, S. Rosato, C. Tamburino, F. Santini, G. Santoro, and F. Seccareccia. Transcatheter aortic valve implantation versus surgical aortic valve replacement for severe aortic stenosis: results from an intermediate risk propensity-matched population of the Italian OBSERVANT study. *Int. J. Cardiol.* 167:1945–1952, 2013.

[14]Ducci A., S. Tzamtzis, M. J. Mullen, and G. Burriesci. Phase-resolved velocity measurements in the Valsalva sinus downstream of a Transcatheter Aortic Valve. In: 16th International Symposium on Applications of Laser Techniques to Fluid Mechanics, Lisbon, Portugal, 9–12 July 2012.

[15]Ge, L., L. Dasi, F. Sotiropoulos, and A. P. Yoganathan. Characterization of hemodynamic forces induced by mechanical heart valves: Reynolds vs viscous stresses. *Ann. Biomed. Eng.* 36:276–297, 2008.

[16]Goubergrits, L. Numerical modeling of blood damage: current status, challenges and future prospects. *Expert Rev. Med. Devices* 3:527–531, 2006.

[17]Goubergrits, L., and K. Affeld. Numerical estimation of blood damage in artificial organs. *Artif. Organs* 28:499–507, 2004.

[18]Grigioni, M., U. Morbiducci, G. D'Avenio, G. Benedetto, and C. Gaudio. A novel formulation for blood trauma prediction by a modified power-law mathematical model. *Biomech. Model. Mechanobiol.* 4:249–260, 2005.

[19]Gross, J. M., M. C. Shu, F. F. Dai, J. Ellis, and A. P. Yoganathan. A microstructural flow analysis within a bileaflet mechanical heart valve hinge. *J. Heart Valve Dis.* 5:581–590, 1996.

[20]Hamdan, A., V. Guetta, E. Konen, O. Goitein, A. Segev, E. Raanani, D. Spiegelstein, I. Hay, E. Di Segni, M. Eldar, and E. Schwammenthal. Deformation dynamics and mechanical properties of the aortic annulus by 4-dimensional computed tomography insights into the functional anatomy of the aortic valve complex and implications for transcatheter aortic valve therapy. *J. Am. Coll. Cardiol.* 59:119–127, 2012.

[21]Hellums, J. D., and C. H. Brown. Blood cell damage by mechanical forces. In: Cardiovascular Flow Dynamics and Measurements, edited by N. H. C. Hwang, and N. A. Normann. Baltimore: University Park Press, 1977, pp. 799–823.

[22]Keane, R. D., and R. J. Adrian. Optimization of particle image velocimeters. I. Double pulsed systems. *Meas. Sci. Technol.* 1:1202, 1990.

[23]Knight, J., V. Kurtcuoglu, K. Muffly, W. Marshall, Jr., P. Stolzmann, L. Desbiolles, B. Seifert, D. Poulikakos, and H. Alkadhi. Ex vivo and in vivo coronary ostial locations in humans. *Surg. Radiol. Anat.* 31:597–604, 2009.

[24]Koos, R., A. H. Mahnken, G. Dohmen, K. Brehmer, R. W. Günther, R. Autschbach, N. Marx, and R. Hoffmann. Association of aortic valve calcification severity with the degree of aortic regurgitation after transcatheter aortic valve implantation. *Int. J. Cardiol.* 150:142–145, 2011.

[25]Koppensteiner, R., A. Moritz, W. Schlick, G. Fenzl, S. Roedler, H. Ehringer, and E. Wollner. Blood rheology after cardiac valve replacement with mechanical prostheses or bioprostheses. *J. Am. Coll. Cardiol.* 67:79–83, 1991.

[26]Leo, H., L. P. Dasi, J. Carberry, H. A. Simon, and A. P. Yoganathan. Fluid dynamic assessment of three polymeric heart valves using particle image velocimetry. *Ann. Biomed. Eng.* 34:936–952, 2006.

[27]Leverett, L. B., J. D. Hellums, C. P. Alfrey, and E. C. Lynch. Red blood cell damage by shear stress. *Biophys. J .* 12:257–273, 1972.

[28]Lim, W. L., Y. T. Chew, T. C. Chew, and H. T. Low. Pulsatile flow studies of a porcine bioprosthetic aortic valve in vitro: PIV measurements and shear-induced blood damage. *J. Biomech.* 34:1417–1427, 2001.

[29]Markl, M., I. Mikati, J. Carr, P. McCarthy, and S. C. Malaisrie. Three-dimensional blood flow alterations after transcatheter aortic valve implantation. *Circulation* 125: 573–575, 2012.

[30]Nobili, M., J. Sheriff, U. Morbiducci, A. Redaelli, and D. Bluestein. Platelet activation due to hemodynamic shear stresses: damage accumulation model and comparison to in vitro measurements. *ASAIO J.* 54:64–72, 2008.

[31]Padala, M., E. Sarin, P. Willis, V. Babaliaros, P. Block, R. Guyton, and V. Thourani. An engineering review of transcatheter aortic valve technologies. *Cardiovasc. Eng. Technol.* 1:77–87, 2010.

[32]Pisani, G., R. Scaffa, O. Ieropoli, E. M. Dell'Amico, D. Maselli, U. Morbiducci, and R. De Paulis. Role of the sinuses of Valsalva on the opening of the aortic valve. *J. Thoracic Cardiovasc. Surg.* 145:999–1003, 2013.

[33]Raffel, M., C. E. Willer, S. T. Wereley, and J. Kompenhans. Particle Image Velocimetry: A Practical Guide. Berlin: Springer, 2007.

[34]Reul, H., A. Vahlbruch, M. Giersiepen, T. Schmitz-Rode, V. Hirtz, and S. Effert. The geometry of the aortic root in health, at valve disease and after valve replacement. *J. Biomech.* 23:181–191, 1990.

[35]Rodes-Cabau, J. Transcatheter aortic valve implantation: current and future approaches. *Nat. Rev. Cardiol.* 9:15–29, 2012.

[36]Saikrishnan, N., S. Gupta, and A. P. Yoganathan. Hemodynamics of the Boston Scientific Lotus™ valve: an in vitro study. *Cardiovasc. Eng. Technol.* 4(4):427–439, 2013.

[37]Saikrishnan, N., C.-H. Yap, N. Milligan, N. Vasilyev, and A. P. Yoganathan. In vitro characterization of bicuspid aortic valve hemodynamics using particle image velocimetry. *Ann. Biomed. Eng*. 40:1760–1775, 2012.

[38]Saikrishnan, N., and A. Yoganathan. Transcatheter valve implantation can alter the fluid flow fields in the aortic sinuses and ascending aorta: an in vitro study. *J. Am. Coll. Cardiol*. 61, 2013. doi:10.1016/S0735-1097(13)61969-5.

[39]Sallam, A. M., and N. H. C. Hwang. Human red blood cells in a turbulent shear flow: contribution of Reynolds shear stresses. *Biorheology* 21:783–797, 1984.

[40]Schultz, C. J., A. Weustink, N. Piazza, A. Otten, N. Mollet, G. Krestin, R. J. van Geuns, P. de Feyter, P. W. J. Serruys, and P. de Jaegere. Geometry and degree of apposition of the corevalve revalving system with multislice computed tomography after implantation in patients with aortic stenosis. *J. Am. Coll. Cardiol*. 54:911–918, 2009.

[41]Shapiro, S. I., and M. C. Williams. Hemolysis in simple shear flows. *AIChE J*. 16:575–580, 1970.

[42]Sheriff, J., D. Bluestein, G. Girdhar, and J. Jesty. High-shear stress sensitizes platelets to subsequent low-shear conditions. *Ann. Biomed. Eng*. 38:1442–1450, 2010.

[43]Sirois, E., and W. Sun. Computational evaluation of platelet activation induced by a bioprosthetic heart valve. *Artif. Organs* 35:157–165, 2011.

[44]Spethmann, S., H. Dreger, S. Schattke, G. Baldenhofer, D. Saghabalyan, V. Stangl, M. Laule, G. Baumann, K. Stangl, and F. Knebel. Doppler haemodynamics and effective orifice areas of Edwards SAPIEN and CoreValve transcatheter aortic valves. *Eur. Heart. J. Cardiovasc. Imaging*. 13:690–696, 2012.

[45]Stühle, S., D. Wendt, G. Houl, H. Wendt, M. Schlamann, M. Thielmann, H. Jakob, and W. Kowalczyk. In-vitro investigation of the hemodynamics of the Edwards Sapien transcatheter heart valve. *J. Heart Valve Dis*. 20:53–63, 2011.

[46]Tzamtzis, S., J. Viquerat, J. Yap, M. J. Mullen, and G. Burriesci. Numerical analysis of the radial force produced by the Medtronic-CoreValve and Edwards-SAPIEN after transcatheter aortic valve implantation (TAVI). *Med. Eng. Phys*. 35(1):125–130, 2013.

[47]Walther, T., and V. Falk. Hemodynamic evaluation of heart valve prostheses: paradigm shift for transcatheter valves? *J. Am. Coll. Cardiol*. 53:1892–1893, 2009.

[48]Wang, X., and X. Li. The influence of wall compliance on flow pattern in a curved artery exposed to a dynamic physiological environment: an elastic wall model versus a rigid wall model. *J. Mech. Med. Biol*. 12:1250079, 2012.

[49]Webb, J. G., and D. A. Wood. Current status of transcatheter aortic valve replacement. *J. Am. Coll. Cardiol*. 60:483–492, 2012.

[50]Wong, D. T. L., A. G. Bertaso, G. Y. H. Liew, V. S. Thomson, M. S. Cunnington, J. D. Richardson, R. Gooley, S. Lockwood, I. T. Meredith, M. I. Worthley, and S. G. Worthley. Relationship of aortic annular eccentricity and paravalvular regurgitation post transcatheter aortic valve implantation with core valve. *J. Invasive Cardiol*. 25:190–195, 2013.

[51]Yap, C. H., H.-S. Kim, K. Balachandran, M. Weiler, R. Haj-Ali, and A. P. Yoganathan. Dynamic deformation characteristics of porcine aortic valve leaflet under normal and hypertensive conditions. *Am. J. Physiol. Heart Circ. Physiol*. 298:H395–H405, 2010.

[52]Yoganathan, A. P., K. B. Chandran, and F. Sotiropoulos. Flow in prosthetic heart valves: state-of-the-art and future directions. *Ann. Biomed. Eng*. 33:1689–1694, 2005.

[53]Young, E., J.-F. Chen, O. Dong, S. Gao, A. Massiello, and K. Fukamachi. Transcatheter heart valve with variable geometric configuration: in vitro evaluation. *Artif. Organs* 35:1151–1159, 2011.